10 Dispersion Engineering: The use of Abnormal Velocities and Negative Index of Refraction to Control the Dispersive Effects

MOHAMMAD MOJAHEDI and GEORGE V. ELEFTHERIADES

The Edward S. Rogers, Sr. Department of Electrical and Computer Engineering, University of Toronto, Toronto, Ontario, Canada

10.1 INTRODUCTION

In recent years two discoveries have led to the possibility of manufacturing materials and structures with dispersive behaviors previously thought unattainable. These are media with an effective negative index of refraction (NIR) also known as the left handed media (LHM) or negative-refractive-index metamaterials [1–4], and the possibility of measuring superluminal [1] or negative group velocities also generically referred to as abnormal group velocities [5–9]. In this manuscript we study the underlying physics and manifestations of these rather unusual behaviors, and will see how a medium can be manufactured that simultaneously demonstrates both properties. But before proceeding, let us describe our motivation behind this approach and see how combining these two effects may lead to the design of new classes of materials with novel and counter-intuitive dispersive effects, a subject we have termed "Dispersion Engineering."

The fact that any physically realizable medium must be dispersive is the consequence of the principle of causality which demands no effect to precede its cause [10]. In the simple case of one-dimensional analysis, the dispersive behavior of a medium can be described by the dependence of the propagation vector on frequency (or equally well

[1]The term superluminal implies group velocities in excess of the speed of light in vacuum.

the dependence of the frequency on the wave vector) according to [11]:

$$\begin{aligned} k(\omega) &= k(\omega_0) + \left.\frac{dk}{d\omega}\right|_{\omega_0} (\omega - \omega_0) + \frac{1}{2}\left.\frac{d^2k}{d\omega^2}\right|_{\omega_0} (\omega - \omega_0)^2 + \ldots \\ &= \nu_p^{-1}\omega_0 + \nu_g^{-1}(\omega - \omega_0) + (1/2)\psi(\omega - \omega_0)^2 + \ldots \end{aligned} \tag{10.1}$$

In Eq. (10.1) the coefficients of expansion ν_p, and ν_g are the phase and group velocities, and ψ is the group velocity dispersion (GVD) given by

$$GVD = \frac{d^2k}{d\omega^2} = -\frac{1}{\nu_g^2}\left(\frac{d\nu_g}{d\omega}\right) \tag{10.2}$$

With the photonic dispersion relation $k(\omega) = \omega\, n_p(\omega)/c$, the dispersive effects of Eq. (10.1) can be also described in terms of the phase index (commonly referred to as the index of refraction, n_p) and its higher order derivatives according to

$$\begin{aligned} k(\omega) &= \frac{\omega}{c} n_p(\omega) \frac{1}{c} \left\{\omega_0\ n_p|_{\omega_0} + n_g\ |_{\omega_0} (\omega - \omega_0)\right. \\ &+ \left. \frac{1}{2}\left[2\frac{dn_p}{d\omega} + \omega\frac{d^2n_p}{d\omega^2}\right](\omega - \omega_0)^2 + \ldots\right\} \end{aligned} \tag{10.3}$$

In Eq. (10.3) the second coefficient of expansion is the group delay which is related to the phase index by

$$n_g = n_p + \omega\, dn_p(\omega)/d\omega. \tag{10.4}$$

The relations between the phase index and phase velocity, group index and group velocity are then as follows:

$$\nu_p = c/n_p(\omega), \tag{10.5}$$

$$\nu_g = c/n_g(\omega). \tag{10.6}$$

So far, in discussing the dispersive effects signified by phase velocity, group velocity, group velocity dispersion, and so on, we have made an implicit assumption that the medium under consideration has a non-negligible spatial extent, or more rigorously $L > \lambda$, where L is the physical length of the one dimensional medium and λ is the wavelength of the excitation. However, the aforementioned dispersive effects can be formulated in a more general way that is equally applicable to both spatially extended ($L > \lambda$) or spatially negligible systems ($L < \lambda$). This formulation relies on the notion of transfer function (impulse response) which can be used to relate the input and the output. The transfer function, also sometimes referred to as the system response or network function, is a complex quantity given by

$$T(\omega) = |T(\omega)|\, exp[j\, \phi(\omega)] \tag{10.7}$$

With a relatively constant value for the transmission function magnitude, or equally well a sufficiently narrow-band excitation, the phase of the transfer function can be expanded in a Taylor series according to

$$\phi(\omega) = \phi(\omega_0) + \left.\frac{\partial\phi}{\partial\omega}\right|_{\omega_0} (\omega - \omega_0) + \frac{1}{2}\left.\frac{\partial^2\phi}{\partial\omega^2}\right|_{\omega_0} (\omega - \omega_0)^2 + \ldots, \tag{10.8}$$

or

$$\phi(\omega) = -\tau_p\omega_0 - \tau_g(\omega - \omega_0) - (1/2)GDD(\omega - \omega_0)^2 + \ldots \tag{10.9}$$

where the phase delay (τ_p), group delay (τ_g), and group delay dispersion (GDD) are given by

$$\tau_p = -\left.\frac{\phi}{\omega}\right|_{\omega_0}, \tag{10.10}$$

$$\tau_g = -\left.\frac{\partial\phi}{\partial\omega}\right|_{\omega_0}, \tag{10.11}$$

$$GDD = -\left.\frac{\partial^2\phi}{\partial\omega^2}\right|_{\omega_0}. \tag{10.12}$$

The connections between the phase and group delays are applicable to both spatially extended and spatially negligible systems [Eqs. (10.11) and (10.12)], and the phase and group velocity (applicable to a spatially extended system, $\lambda > L$) is then as follows

$$\nu_p = \frac{c}{n_p(\omega)} = \frac{L}{\tau_p}, \tag{10.13}$$

$$\nu_g = \frac{c}{n_g(\omega)} = \frac{L}{\tau_g}, \tag{10.14}$$

In fact, Eq. (10.14) can be obtained using more rigorous arguments based on the Fourier transform theorem [12], or more intuitively by considering the wave propagation through a slab of thickness L , matched to its surrounding media (i.e. no reflection at the interfaces), having the transmission function $T = exp(j\phi) = exp[-j\,k(\omega)\,L]$. Finally, two more points are worth mentioning. First, from Eq. (10.14) it is clear that for a physical system of length L the sign of the group velocity and group delay are the same. Second, when discussing a spatially extended system, the fundamental requirements of causality, also referred to as "primitive causality," must be augmented with relativistic causality, also referred to as "macroscopic" or "Einstein causality" [13]. We note that the concept of primitive causality is more general than macroscopic causality since it does not rely on the existence of a finite speed (c) for propagation of the "cause."

Now, the notion of "Dispersion Engineering" alluded to earlier, reflects our desire to synthesize and control various dispersive effects, and in particular their associated

signs, as manifested by the phase delay, group delay, group delay dispersion, and so on (see Eq. (10.9) or similarly Eqs. (10.1) or (10.3)). In the remaining parts of this manuscript we focus only on the first two terms of the expansion, i.e. the phase and group delays or equally well the phase and group velocities and leave the consideration of the group delay dispersion to later times.

From a physical point of view, the phase and group delays are the delays encountered by sinusoidal time harmonics and the wave packet envelope (composed of such harmonics) as they propagate through the media, respectively. Under usual propagation conditions, both the phase and group velocities (read phase and group delays) are positive, indicating the fact that both the sinusoidal time harmonics and the pulse envelope move away from the source.

In the case of negative phase but positive group velocity (read negative phase but positive group delays) the sinusoidal time harmonics move toward the source while the wave packet envelope moves away from the source. This phenomenon is sometimes referred to as backward wave propagation [14] and is the signature of the LHM studies so far [4, 15–17].

More interestingly, under some conditions, it is also possible to observe positive phase but negative group velocities (read positive phase but negative group delays) [18–21]. Under these circumstances, for a finite length medium exhibiting such abnormal behavior and illuminated by a source outside, the observer will note that the sinusoidal time harmonics move away from the source but the wave packet envelope (inside the medium) moves toward the source. Stated otherwise, our observer will note that the peak (envelope) of a well-behaved pulse will emerge from the medium prior to the peak of the incident pulse entering it. This counter intuitive behavior is a subclass of the so called "abnormal group velocities" which will be revisited shortly in the next section.

Finally, by combining the backward waves and abnormal group velocities one can synthesize a medium with simultaneous negative phase and group velocities (read negative phase and group delays.) Under this condition, both the sinusoidal time harmonics and the wave packet envelope move toward the source. This case is of particular interest to us and will be investigated theoretically and experimentally in the following sections.

In Sec. 10.2 we revisit the concept of abnormal group velocities (superluminal or negative) and will provide a short overview of the field. We begin our study of the NRI media exhibiting both negative phase and negative group velocities with the simple case of slab having a Lorentzian magnetic and electric response. This simple case will set the stage for more detailed analysis of NRI media realized by periodically loading a transmission line which exhibits both negative phase and group delays. The theoretical and experimental studies of such media can be found in Sec. 10.4. For the sake of brevity the results of similar observations in a LHM consisted of split-ring resonator (SRR) and strip wires will be presented elsewhere, whereas an interested reader may consult Ref. [22] for a brief description of this situation. Finally, we summarize our work in Sec. 10.5.

10.2 ABNORMAL GROUP VELOCITY

Soon after Einstein's formulation of special relativity in 1905, the question of wave propagation in a medium with Lorentz-Lorenz dispersion captured the attention of the researchers of the time [23]. It was known, at least theoretically, that within the region of anomalous dispersion for such medium the group velocity — describing the velocity by which the peak and hence the envelope of a well behaved wave packet travels — can exceed the speed of light in vacuum, i.e. it becomes superluminal. On its face value, this theoretical possibility was in contrast with the requirements of relativistic causality as formulated by Einstein. Sommerfeld and then his post doctoral fellow, Brillouin, undertook the analysis of this problem, the result of which was published in 1914 and later republished and expanded in Ref. [23]. The two authors defined or clarified many velocity terms such as phase, group, energy, "signal[2]," and most importantly the first and second forerunner (precursor) velocities. One important aspect of their work was establishing the fact that the velocity of the earliest field oscillations known as the front will never exceed the speed of light in vacuum; and in fact, under all circumstances it remains exactly luminal. While this seminal work confirmed the compatibility of the relativistic causality and wave propagation in a Lorentzian medium; nevertheless Brillouin along with many others considered the superluminal or negative group velocities as unphysical, and perhaps a mere mathematical consideration [24–26].

Decades later, in 1970, Garret and McCumber revisited the same problem and concluded that under certain easily satisfied conditions, superluminal or negative group velocities may be observed and are therefore physical [27]. In their work, they considered the propagation of Gaussian packets and showed that these could travel at abnormal group velocities without significant distortion of the pulse shape even though the pulse was attenuated.

Chu and Wang (1982) were the first to experimentally demonstrate the existence of abnormal group velocities for picosecond laser pulses propagating through the excitonic absorption line of a GaP:N sample [28]. Since then, abnormal group velocities have been measured in various structures including photonic crystals, undersized waveguides, misaligned horn antennas, side by side prisms, and inverted media [6, 8, 20, 21, 29–33].

Figure 10.1 summarizes the results. Consider a medium of length L, excited from left by a smoothly varying pulse (such as Gaussian or Sinc). The pulse on the right is the transmitted pulse (output.) Under normal propagation conditions the medium group index [see Eq. (10.4)] is greater than one, which implies a group delay larger than L/c and a group velocity less than c. In other words, the output pulse peak (envelope) is delayed as compared to the input. On the other hand, for $0 < n_g < 1$, the group

[2]The "signal" velocity as defined by Sommerfeld and Brillouin is approximately the velocity of the half-maximum point, and by their own admission is an arbitrary construct. In other words, in light of new observations of abnormal velocities, the so called "signal" velocity should not be confused with genuine information velocity which is constrained by relativistic causality.

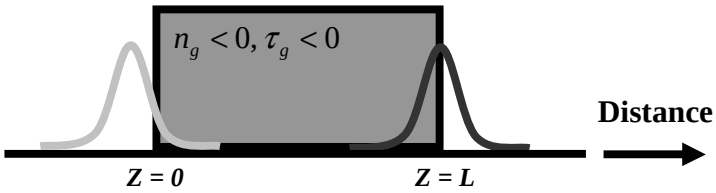

Fig. 10.1 A well-behaved wave packet incident from left and traveling through a medium of length L.

velocity is larger than c and the group delay is less than L/c. This is the case of superluminal group velocity. When the group index approaches zero ($n_g \to 0$), the group velocity grows unbounded ($\nu_g \to \infty$) and the group delay approaches zero ($\tau_g \to 0$). To the observer, the peak of the output pulse in Fig. 10.1 appears at the right interface ($z = L$) at the same time the peak of the input wave packet is at the left interface ($z = 0$). Now, if we continue with our analysis and consider a negative group index ($n_g < 0$), then both the group velocity and group delay are also negative ($\nu_g < 0, \tau_g < 0$). Under this condition, the observer notes that the peak of the output leaves the medium prior to the peak of the input entering it, as it is depicted in Fig. 10.1.

While Fig. 10.1 depicts the pulse propagation in space, better insight may be obtained by considering the behavior in time. Figure 10.2 shows the abnormal wave propagation in the time domain. The picture is equally applicable to both cases of superluminal or negative group velocities. Whereas, in the later case the input and output are to be understood as the input to and output from the medium of length L (depicted in Fig. 10.1), in the former case the input is to be understood as a wave packet traveling a distance L through vacuum and the output is a pulse traveling through a medium of the same length with $0 < n_g < 1$. There are two points worth emphasizing.

First, for the passive medium, the superluminal or negative group velocity is accompanied by attenuation of the pulse. In other words, for such a medium, the wave packets depicted in Fig. 10.2 are considered to be normalized to their respective maximum values. However, such attenuation is not a necessary condition for all cases of abnormal group velocities. In fact, it has been shown that an inverted medium (a medium with gain) can display abnormal group velocities without attenuation [18–21, 34].

Second, as Fig. 10.2 shows, and discussed in more details in sections 10.4.4.2 and 10.4.4.3, while the peak of the output precedes the input peak, the earliest part of the output pulse — presented by a discontinuity in the envelope or higher order derivatives of the envelope — is retarded with respect to the input. In other words, while the peak of the output is advanced in time, its front is not. In this sense, the "genuine information" conveyed by our electromagnetic pulse (for example, a "1" or

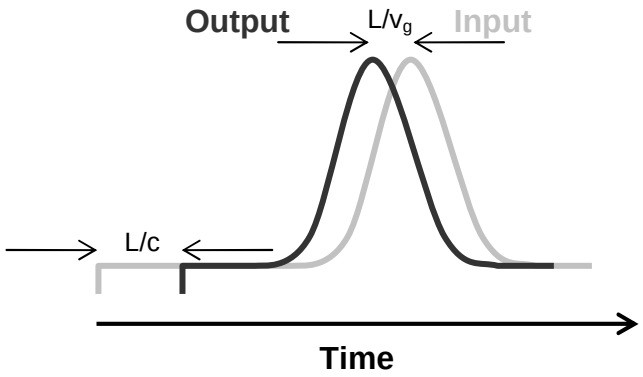

Fig. 10.2 The input and output wave packets. The output pulse travels with superluminal or negative group velocities, while its front (the discontinuity) propagates at luminal speed.

a "0") is carried by the points of non-analyticity (discontinuities) [8,9] and therefore from the theoretical point of view there is no contradiction between the behavior depicted in Fig. 10.2 and the requirements of causality. It must be added that for a Lorentzian medium, the oscillation frequency of the points of non-analyticity (front) is extremely high while their associated amplitude is very low; hence, from a practical point of view, the detection of the front and precursor fields may not be the most convenient scheme for routine detection of signals.

10.3 WAVE PROPAGATION IN A SLAB WITH NEGATIVE INDEX OF REFRACTION

A brief review of current literature shows that the meaning of negative group velocity and its connection with LHM is mired by misunderstandings and misconceptions [2, 4, 35, 36]. The subject of negative group velocity in such media is of particular interest, since most theoretical and experimental studies presented so far only consider the case of anti-parallel phase and group velocities (backward waves) for which the group velocity is positive and points away from the radiating source, while the phase velocity is negative and points toward the source [3,4,15,36]. To begin our discussion of negative group velocity and group delay in LHM, we start with the simple case of a slab with simultaneous negative permittivity and permeability.

The medium is characterized by [3]

$$\epsilon = 1 - \frac{\omega_{ep}^2 - \omega_{eo}^2}{\omega^2 - \omega_{eo}^2 - j\gamma_e\omega} \tag{10.15}$$

and by

$$\mu_{eff} = 1 - \frac{\omega_{mp}^2 - \omega_{mo}^2}{\omega^2 - \omega_{mo}^2 - j\gamma_m\omega} \tag{10.16}$$

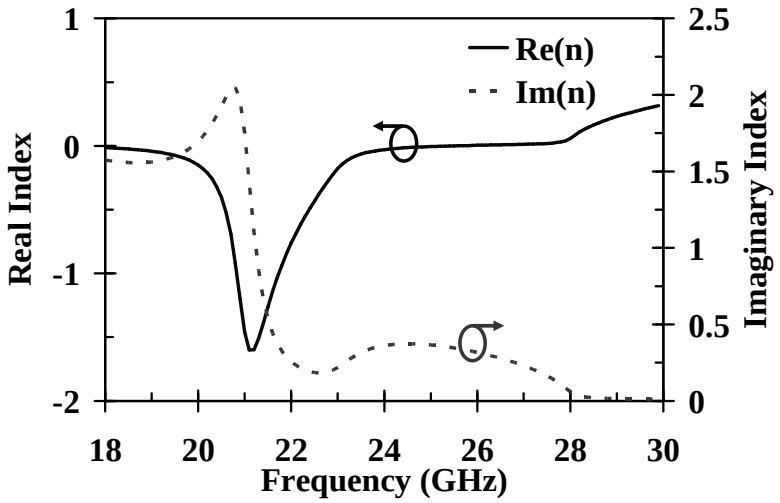

Fig. 10.3 The real and imaginary parts of the index of refraction. ω_{eo} = 0 GHz, ω_{ep} =2$\pi\times$ 28 GHz, ω_{mo} = 2$\pi\times$ 21 GHz, ω_{mp} = 2$\pi\times$ 23 GHz. γ_e = 1.6 $\times$ 10^9 s^{-1}, and γ_m = 4 $\times$ 10^9 s^{-1}.

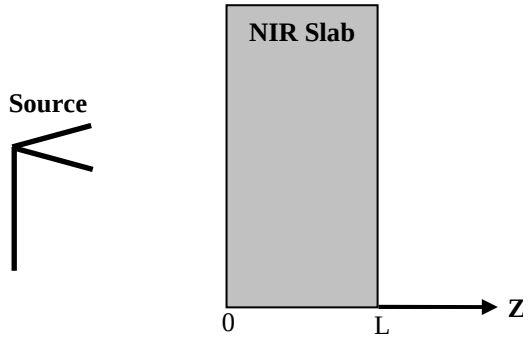

Fig. 10.4 A slab with NIR irradiated by a source to its left

where ω_{ep}, ω_{mp} are the electric and magnetic plasma frequencies and ω_{eo}, ω_{mo} are the electric and magnetic resonance frequencies respectively. The γ_e and γ_m are the phenomenological electric and magnetic damping constants. In regions for which the real parts of the effective permeability and permittivity are both negative, the index of refraction is also negative [4]. Figure 10.3 shows the real and imaginary parts of the effective index calculated from $n_{eff} = \sqrt{\epsilon_{eff}}\sqrt{\mu_{eff}}$.

Figure 10.4 shows the geometry of the problem under consideration. A slab of thickness L with dispersion characteristics depicted in Fig. 10.3 is irradiated by plane waves from a source located to its left at negative z-values. The transmission

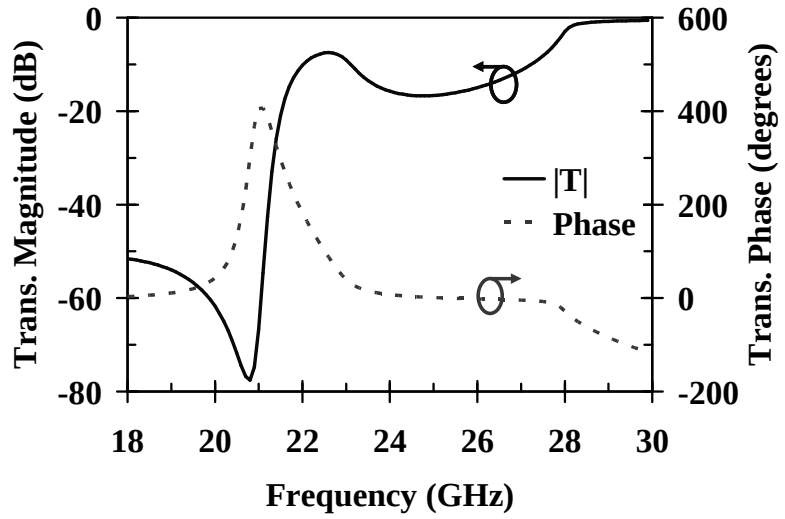

Fig. 10.5 Transmission magnitude and phase for a 1 cm thick section of NIR medium. All material parameters are the same as in Fig. 10.3.

coefficient (magnitude and phase) can then be calculated according to

$$T(\omega) = \frac{t_{12}t_{23}e^{-jk_2L}}{1 + r_{12}r_{23}e^{-j2k_2L}} = |T(\omega)|\, e^{j\phi}, \tag{10.17}$$

where $t_{i,j}$ and $r_{i,j}$ are the Fresnel transmission and reflection coefficients corresponding to the slab boundaries and k_2 is given by

$$k_2 = \frac{2\pi}{\lambda} n_2 \cos\theta_2. \tag{10.18}$$

In the following we assume that the NIR medium is surrounded by vacuum ($n_1 = n_3 = 1$) and is illuminated at normal incidence ($\theta_1 = 0$).

Figure 10.5 shows the transmission function (magnitude and phase) for a left handed slab, 1 cm thick. Note that in the vicinity of minimal transmission, corresponding to the region of anomalous dispersion, the slope of the transmission phase changes sign, implying a change of the sign for the group delay and group velocity.

The group delay and the real part of the index are plotted in Fig. 10.6. From the figure it is evident that group delay and hence the group velocity are negative within the region of anomalous dispersion and are positive away from it. Note that the real part of the index is negative from 18 to 25.4 GHz, while at the frequency $\nu_t = 21.2$ GHz the group delay changes sign from negative to positive.

This implies that for frequencies greater than ν_t the group velocity is positive, whereas the phase velocity remains negative, corresponding to the backward wave propagation discussed earlier. The fact that the group velocity is positive for frequencies greater

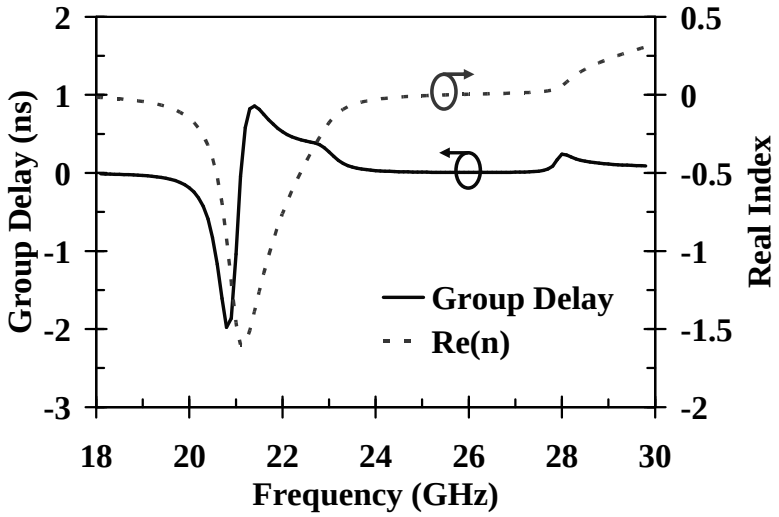

Fig. 10.6 Group delay and real part of the index for a 1 cm thick section of NIR medium. All material parameters are the same as in Fig. 10.3.

than ν_t, can also be seen from the behavior of the index of refraction in Fig. 10.6. In this frequency range $\omega\, dn/d\omega$ is positive and larger than n, indicating a positive value for the group velocity calculated from [3]

$$V_g = \frac{c}{n + \omega\, dn/d\omega} = \frac{c}{n_g} \tag{10.19}$$

where n_g is the group index. The existence of regions of negative group/negative phase velocities, and positive group/negative phase velocities (backward waves) for the above case can also be verified using full-wave simulations.

From the above discussions it is clear that LHM, similar to right-handed-media (RHM), possesses an anomalous dispersion region in which the group velocity is negative. However, the LHM anomalous dispersion region differs from that of RHM in at least two respects. First, in the case of LHM, the negative group velocity is also accompanied with a negative phase velocity. Second, at the minimal dispersion point ($dn/d\omega = 0$) or frequency interval for which $dn/d\omega \approx 0$ the LHM exhibits a group velocity given by

$$V_g \approx V_p = \frac{c}{n} < 0, \tag{10.20}$$

which is negative, in contrast to the case of LHM.

[3]Eq. (10.19) assumes perfect matching between the slab and the surrounding media, i.e. $r_{12} = r_{23} = 0$. The effects of mismatches (interfaces) which produce negligible positive delays will not alter the conclusions presented above. Note that Eq. (10.11) which is used to plot the group delay in Fig. 10.6 takes into account the positive delays associated with the interfaces.

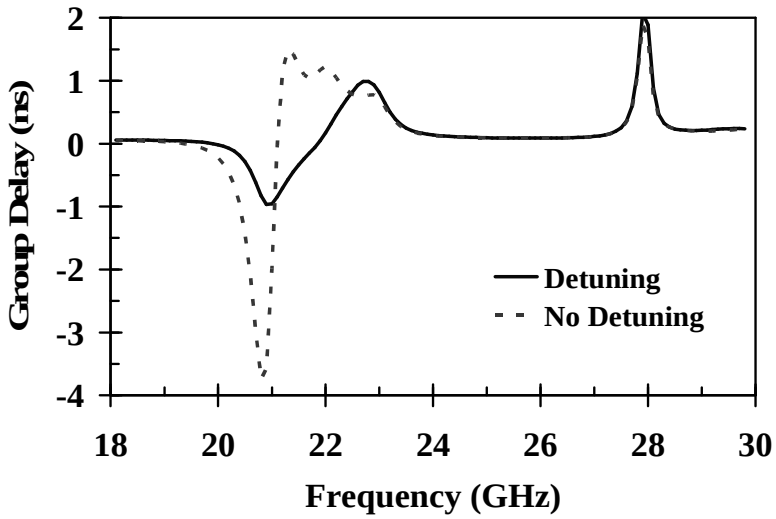

Fig. 10.7 Group delay for detuned (solid curve) and non-detuned (dashed curve) 1DPC with 8 LHM slabs separated by air

Finally, note that negative refractive index is an artificial dispersion in which the characteristics of the underlying sub-wavelength unit cell control the overall dispersive behavior. It is then possible to slightly vary the frequency response of each unit cell (detuning) in order to broaden the frequency range over which negative phase and group delays are exhibited. As a proof of concept Fig. 10.7 shows the group delays for a one-dimensional photonic crystal (1DPC) consisting of 8 RHM slabs separated by air. For the detuned structure (solid curve), the magnetic resonance of each slab is increased by 1 GHz as compared to the previous layer — starting with $\omega_{mo} = 21$ [GHz] for the first slab — while keeping all other parameters the same as before. The figure also shows the group delay for the 1DPC without detuning (dashed curve.) As a result of detuning, the negative group delay bandwidth in Fig. 10.7 has increased from 1.7 GHz to 2 GHz (an increase of 18%) while the absolute value of negative group delay has decreased (from -3.7ns to -0.97ns). The above tradeoff between the bandwidth and the amount of negative delay is a fundamental design constraint.

10.4 PERIODICALLY LOADED TRANSMISSION LINE WITH AN EFFECTIVE NEGATIVE INDEX OF REFRACTION AND NEGATIVE GROUP INDEX

In the previous section we discuss the ideal, but not practical, case of a slab or multiple slabs having an effective negative index of refraction. Here, we concentrate on the actual structures that are manufactured to exhibit such responses. We begin with the general theory of the periodically loaded transmission line (PLTL) and show

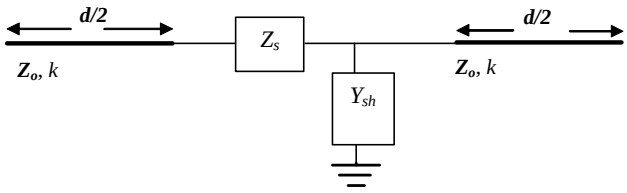

Fig. 10.8 A unit cell of a transmission line loaded with lumped series impedance Z_s and shunt admittance Y_{sh}.

how such a device can be modified in order to exhibit combinations of positive or negative phase and group delays.

10.4.1 General Theory of PLTL Exhibiting Negative Phase Delay

Figure 10.8 shows the unit cell of a transmission line repeatedly loaded with lumped series impedance (Z_s) and shunt inductance (Y_{sh}). This periodic structure can be considered as an effective medium, provided that the dimensions of the unit cell are small as compared to the excitation wavelength. The study of such PLTL with the help of a dispersion diagram is a subject well examined in electromagnetic theory [37, 38] and will be used in our analysis.

The loading elements Z_s, and Y_{sh} can be chosen such that the overall result is a medium exhibiting backward wave propagation, i.e. a medium with an effective negative index of refraction. This approach in designing a medium with backward wave propagation (negative phase velocity) is well described in other chapters of this book and will not be repeated here. We suffice by stating that a two dimensional version of such PLTL has been used to demonstrate focusing of a radiating cylindrical source [15].

10.4.2 PLTL Exhibiting Negative or Positive Phase and Group Delays - Frequency Domain Simulations

For the PLTL discussed in section 10.4.1 the loading elements Z_s and Y_{sh} can be chosen such that the resulting structure exhibits both negative group delay (negative group velocity) and negative phase delay (negative phase velocity). Figure 10.9 shows the unit cell of such a PLTL [39]. Using the ABCD transmission matrix, the complex propagation constant (γ) of the periodic structure is given by

$$\cosh \gamma d = \cos[(\alpha + j\beta)d] = \cos kd + j\frac{(Z_s + Y_{sh}Z_0^2)}{2Z_0}\sin kd + \frac{Z_s Y_{sh}}{2}\cos kd \tag{10.21}$$

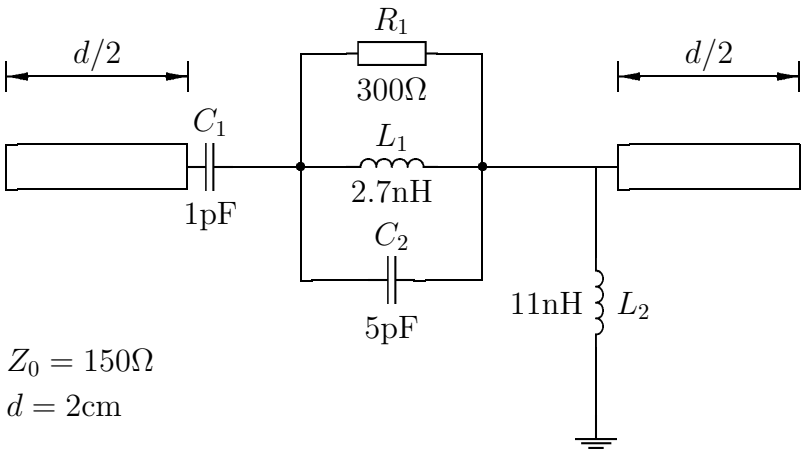

Fig. 10.9 Unit cell of the proposed loaded transmission line which exhibits negative refractive index as well as negative group delay. Typical component values are also shown

Here, α and β are the attenuation and phase constants of the periodically loaded medium, whereas, k, Z_0, and d are the propagation constant, the characteristic impedance, and the length of the unit cell for the unloaded line, respectively.

In order for our PLTL to exhibit a region of anomalous dispersion with negative group delay in addition to negative phase delay (an effective negative index), the line is loaded in series with capacitor C_s and an $R_r L_r C_r$ resonator, and in shunt with an inductor L_{sh} [40]. The series impedance (Z_s) and shunt admittance (Y_{sh}) of (10.21) are then given by

$$Z_s = \frac{1}{j\omega C_s} - \frac{j\omega \frac{1}{C_r}}{\omega^2 - j\omega \frac{1}{R_r C_r} - \frac{1}{L_r C_r}}, \tag{10.22}$$

$$Y_{sh} = \frac{1}{j\omega L_{sh}}. \tag{10.23}$$

Note that the resonant frequency of the parallel $R_r L_r C_r$ resonator, $f_0 = 1/2\pi\sqrt{L_r C_r}$, is also approximately the center frequency of the region of anomalous dispersion.

Figure 10.10 (solid curve) shows the dispersion diagram of the proposed periodic structure. The component values used to produce the curves are indicated in Fig. 10.9. The characteristic impedance of the unloaded line used in the simulation is 150 Ω and the length of the unit cell (d) is 2 cm. The first pass-band extends from frequency f_1 to f_4 which also spans the region of anomalous dispersion ($f_2 < f < f_3$). The second stop-band ($f_4 < f < f_5$) and second pass-band ($f > f_5$), along with the appropriate signs for the phase and group velocities in each branch are also shown.

Figure 10.10 indicates that within the first pass-band ($f_1 < f < f_4$) branches marked I and II can describe the wave propagation in our PLTL. A question then can be

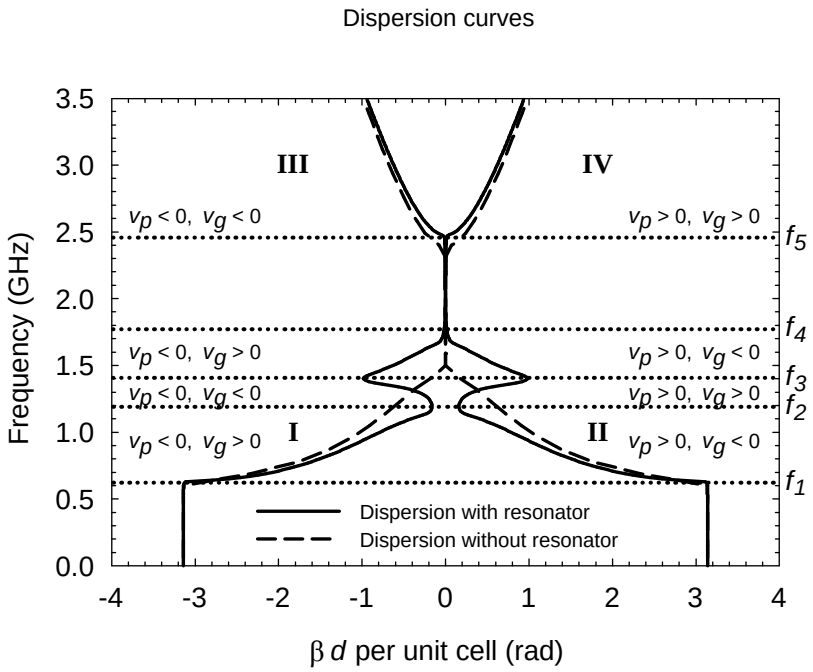

Fig. 10.10 Dispersion diagram (solid curve) of the proposed transmission line medium exhibiting simultaneous negative refractive index and negative group velocity in the first pass-band. Dotted curve shows the dispersion of the periodic medium without the $R_r L_r C_r$ resonators.

asked. Which of the two branches correctly describes the wave propagation through the structure? To answer this we may consider the following. First, the dashed curve in Fig. 10.10 shows the dispersion relation for a transmission line without the $R_r L_r C_r$ resonant circuit. As stated in section 10.4.1 and described in Ref. [15], such a transmission line has been shown to exhibit an equivalent negative index of refraction, i.e., a negative value for βd, which designates the branch-I as the appropriate choice. We may now consider the presence of the $R_r L_r C_r$ resonator as a perturbation to the previously studied case, and as such we once again must choose branch-I as our dispersion curve. Second, the difference in the insertion phase for two transmission lines with different lengths can be used to deduce the proper branch. This point is discussed in the next section, and again it is seen that branch-I correctly describes the wave propagation in our PLTL. Finally, we should note that within the second pass-band ($f > f_5$), the dispersive behavior depicted by the branch-IV properly describes the wave propagation for our PLTL.

At this point, a few remarks regarding the relative signs of the phase and group velocities are in order. As Fig. 10.10 shows, for branch-I, and within the frequency range $f_1 < f < f_2$ the phase and group velocities are anti-parallel (have opposite signs). This traditionally describes backward-wave propagation [14] and is the regime under which the theoretical and experimental work in references [3, 15, 36] were carried out. The frequency range $f_2 < f < f_3$ of branch-I corresponds to the region of anomalous dispersion for which the phase and group velocities are parallel and are both negative. This frequency interval designates a band for which the term negative group velocity can be correctly used in connection with NRI metamaterials. The frequency range $f_3 < f < f_4$ is once again the region of backward wave propagation, whereas for $f > f_5$ in branch-IV, the PLTL behaves as a normal medium with parallel and positive phase and group velocities.

To properly describe the wave propagation through a finite length PLTL, a unit cell of which was shown in Fig. 10.9, we will use the scattering matrix formulation. In order to closely emulate the experimental results of the next section, we will monotonically increase the number of unit cells from one to four and terminate the transmission line with a 50 Ω impedance.

Figures 10.11(a) and 10.11(b) show the S_{21} (transmission function) magnitude and phase for the PLTL as the number of unit cells is increased. The frequency bands corresponding to the first and second pass-bands and stop-bands along with the region of anomalous dispersion are also displayed. As expected, within the region of anomalous dispersion ($f_2 < f < f_3$), the transmission magnitude is minimal, and it is within this frequency band that the negative group delay is to be observed [18]. Figure 10.11(b) shows the unwrapped transmission phase for the same range of frequencies. From the figure it is clear that within the region of anomalous dispersion ($f_2 < f < f_3$) the derivative of the phase function (ϕ) reverses its sign, hence implying the existence of a negative group delay and group velocity.

The fact that our PLTL, within the frequency bands $f_1 < f < f_4$, exhibits an equivalent negative index of refraction can also be verified from Fig. 10.11(b).

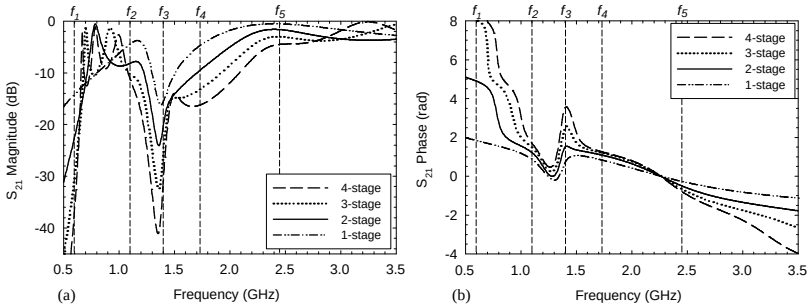

Fig. 10.11 (a) Calculated $|S_{21}|$ for the PLTL of Fig. 10.9 with different number of stages. (b) Calculated unwrapped S_{21} phase for the same transmission line with different number of stages.

Assuming an unbounded medium, i.e. neglecting the mismatches [4], the difference between the insertion phases of two PLTLs of lengths d_1 and d_2 is given by

$$\Delta\phi = \phi_2 - \phi_1 = \frac{\omega\, n(\omega)}{c}(d_2 - d_1). \tag{10.24}$$

Note that for $d_2 > d_1$ and normal media ($n > 0$), the difference in the insertion phase calculated from (10.24) is negative ($\Delta\phi < 0$), whereas from Fig. 10.11(b), in the frequency band $0.5 < f < 2.3$ GHz, it is positive indicating an equivalent negative refractive index. Interestingly, as Fig. 10.11(b) implies, for the second pass-band ($f > 2.3$ GHz) $\Delta\phi$ is negative implying a normal transmission line operation. Finally, we expect that as the number of stages increases, the finite length PLTL more closely approximates the dispersion characteristics of infinitely long PLTL depicted in Fig. 10.10.

Figure 10.12 shows the calculated group delay [Eq. (10.11)] for our PLTL with 1, 2, 3, and 4 unit cells. In accordance with the results for an infinitely long PLTL depicted in Fig. 10.10, it is seen that for a finite length PLTL, the group delay is negative within the frequency band $f_2 < f < f_3$, and is positive away from the anomalous dispersion region. It must be noted that as the length of the finite length PLTL is increased, the amount of negative delay (in absolute value sense) is also increased. In other words, longer transmission lines produce more time advances (negative delays) as compared to shorter lines, however, at the cost of reducing the transmitted signal amplitude. In the next section a frequency-domain setup is used to verify these theoretical predictions.

[4] Including effects of the boundaries (mismatches) only complicates the calculations but will not change the final conclusions.

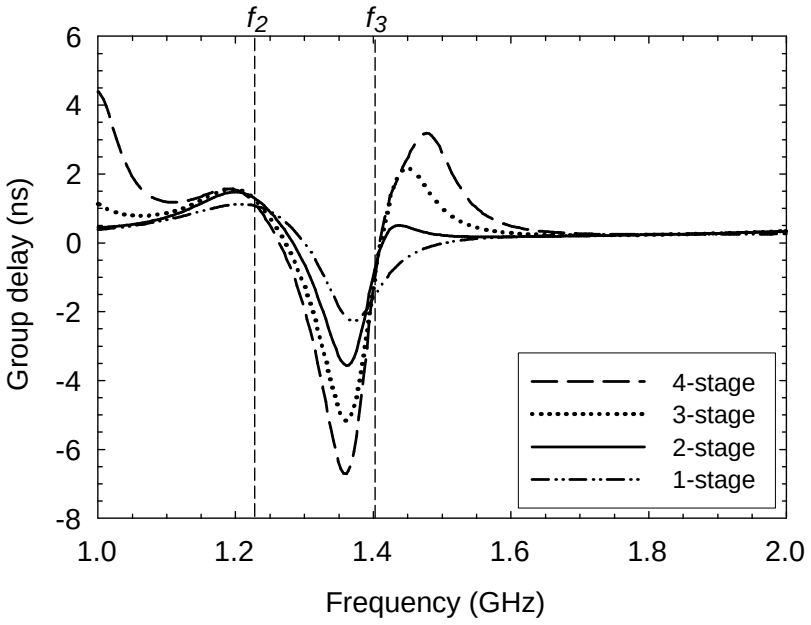

Fig. 10.12 Calculated group delay for the PLTL of Fig. 10.9 with 1, 2, 3, and 4 stages. Figure only shows the region of anomalous dispersion and its vicinity.

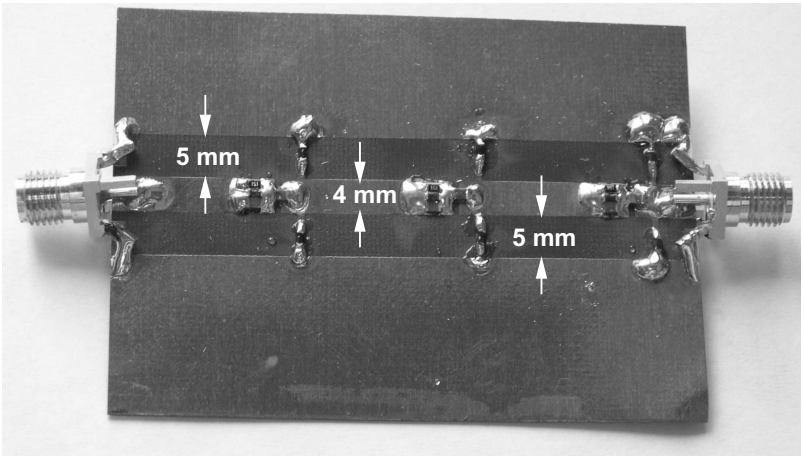

Fig. 10.13 PLTL with 3-stages. The board is Rogers 5880 with a substrate thickness of 0.381 mm, a relative permittivity of 2.2, a loss tangent of 0.0009, and volume and surface resistivities of 2×10^7 MΩ·cm and 3×10^8 MΩ, respectively. The copper cladding thickness is 17 μm. The center conductor of the waveguide has a width of 4 mm and the slots have a width of 5 mm.

10.4.3 PLTL Exhibiting Negative or Positive Phase and Group Delays - Frequency Domain Measurements

To verify our theoretical predictions, a coplanar waveguide (CPW), printed on Rogers 5880 substrate with dielectric constant of 2.2 and thickness of 0.381 mm, was designed. The CPW line was periodically loaded with surface-mounted chips of size 1.5 mm by 0.5 mm, such that one unit cell was approximately 2 cm long. To perform the experiment, PLTLs with 1, 2, 3, and 4 unit cells were fabricated. Figure 10.13 shows a PLTL with 3 stages. The device was connected to a vector network analyzer (HP-8722C), and in order to measure the transmission function (S_{21}) a full two-port calibration was performed.

The magnitude and phase of S_{21} are displayed in Figs. 10.14(a) and 10.14(b) respectively. The stop-, pass-, and the anomalous dispersion bands are also shown.

Figure 10.14(a) clearly indicates that, in accordance with the theoretical predictions of the previous section, as the number of unit cells is increased, the magnitude of the insertion loss also increases. Furthermore, as discussed earlier, Fig. 10.14(b) shows that in the frequency band $f_1 < f < f_4$ the phase differences ($\Delta\phi$) between two PLTLs of different lengths ($d_2 > d_1$) are positive, implying that the PLTLs exhibit an effective negative index of refraction. On the other hand, for $f > f_4$, $\Delta\phi$ is negative, indicating a normal transmission line behavior. Finally, in Fig. 10.14(b) the region of anomalous dispersion ($f_2 < f < f_3$) can be identified by the reversal of the slope.

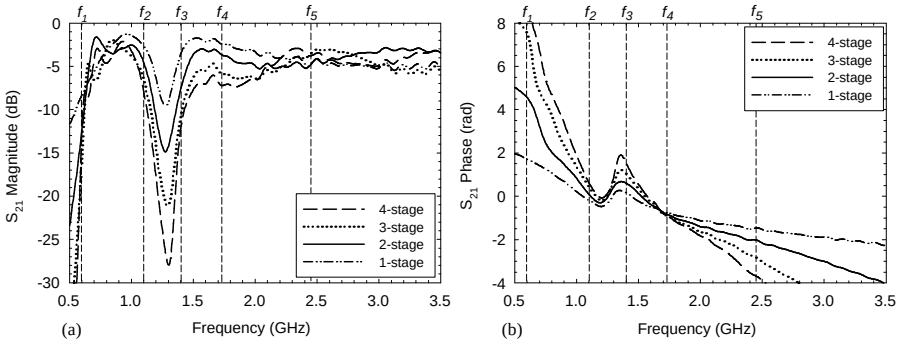

Fig. 10.14 (a) Measured S_{21} magnitudes of the PLTLs with one, two, three, and four unit cells. (b) Measured unwrapped S_{21} phases of the same PLTLs.

While the overall agreement between the theoretical predictions of Figs. 10.11(a) and 10.11(b) and the experimental results of Figs. 10.14(a) and 10.14(b) is good, in general, a shift of 50 to 80 MHz can be detected. For example, the experimental value for the center frequency of the region of anomalous dispersion is 1.29 GHz, whereas the theoretically predicated value is approximately 1.37 GHz. Moreover, around the resonances, more losses are predicted by the simulations as compared to the experimental results.

These discrepancies can be accounted for by considering a few factors. First, in all of our simulations we have used the nominal values associated with the surface-mount lumped elements provided by the manufacturer. Our experience has shown that in many cases, in part due to the embedded parasitics, the actual measured values can be significantly different. Second, in our simulations the resistance and conductance associated with the inductor L_r and the capacitor C_r have been ignored. The effect of this series resistance for the inductor and conductance for the capacitor is to reduce the overall impedance of the parallel $R_r L_r C_r$ resonant circuit, hence reducing the theoretically predicted insertion losses. Third, for the PLTLs with more than one stage, the resonant frequency for each stage is slightly different from the others due to variations in the component values. This non-homogeneity was not taken into account in our theoretical model and in practice it broadens the anomalous dispersion region, thus reducing the overall measured insertion losses in addition to decreasing the slope of the phase within this region.

The group delay for each truncated PLTL is shown in Fig. 10.15. The frequency band of interest is the anomalous dispersion region ($f_2 < f < f_3$) in which the group delay is more negative for longer transmission lines. The measured maximum group delay for the four stage PLTL is approximately -4ns compared to -7ns obtained from the simulations. This difference is attributed to the decrease in slope of the transmission phase as discussed above.

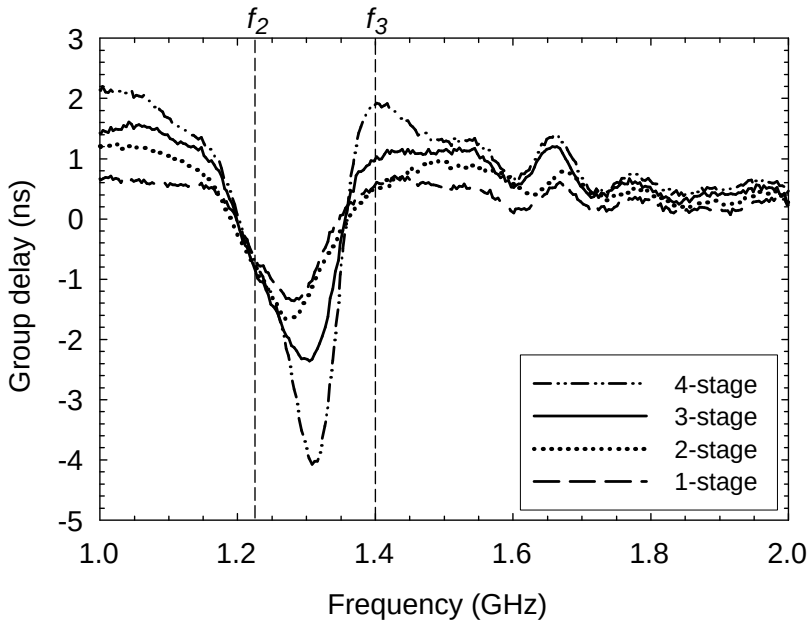

Fig. 10.15 Measured group delay for the PLTL with 1, 2, 3, and 4 unit cells. Larger negative delays (in absolute sense) are measured for longer transmission lines.

10.4.4 PLTL Exhibiting Negative or Positive Phase and Group Delays - Time Domain Simulations

In our discussion of Sec. 10.1 we observed that the phase delay is the delay associated with underlying sinusoidal harmonics, whereas the group delay is the delay of the pulse envelope. In a system supporting negative phase delay the output sinusoidal harmonics lead the input, while in a system with negative group delay, the peak of the output wave packet precedes the peak of the input wave packet. In this section, we theoretically and experimentally study these effects directly in the time-domain [41]. Since the concept of negative phase delay (phase lead) is well understood within standard circuit analysis, we spend most of our time describing the negative group delay for structures supporting both behaviors. We start our discussion with simulating a PLTL which exhibits negative or positive phase or group delays depending on the frequency of operation and show how despite the counter intuitive shift of the pulse envelope to earlier times Einstein's causality is not violated.

10.4.4.1 Negative Group Delay In order to study time-domain behavior of our PLTL, three loaded CPW transmission lines with unit cells depicted in Fig. 10.9 were considered. The only difference between the unit cell studied here and the one discussed in sections 10.4.2 and 10.4.3 is that the value of R_r was reduced from 300 Ω to 150 Ω. The total lengths of the lines with one, two, and three unit cells were 2, 4 and 6 cm respectively. The transmission lines were excited with Gaussian pulses of temporal length 30 ns, modulated at the resonance frequency of the series $R_rL_rC_r$ loading element (1.3 GHz). Using the specification sheet for the Rogers 5880 samples with conductor thickness of 17 μ m, the substrate and conductor losses were included in our analysis, whereas the lumped components used in the simulation were assumed to be ideal.

The simulations were performed using Agilent's Advanced Design System (ADS), where Fig. 10.16 shows the calculated voltage waveforms at the input and output of the loaded lines. The peaks of all three output pulses *precede* the input peaks by an amount proportional to the length of the line. In other words, since the longer lines have more unit cells, they generate a larger negative group delay. This negative delay is mostly due to the series $R_rL_rC_r$ resonator and thus resonant absorption losses are also introduced, as indicated by the drop in magnitude of the output voltage waveforms. For example, in the case of the 2-cm transmission line, a negative delay of -0.89 ns is predicted while the output voltage peak is approximately 15 percent of the input. Note that some of the predicted losses are due to mismatched impedances between the loaded transmission line (150 Ω) and the source (50 Ω).

10.4.4.2 Luminal Front Velocity Figure 10.16 shows that the pulse peak and envelope propagate with a negative group delay and consequently the pulse travels with a negative group velocity. Contrary to the traditional point of view, negative and superluminal group velocities are therefore physical and measurable, and do not contradict the requirements of relativistic causality. While a rigorous analysis of this

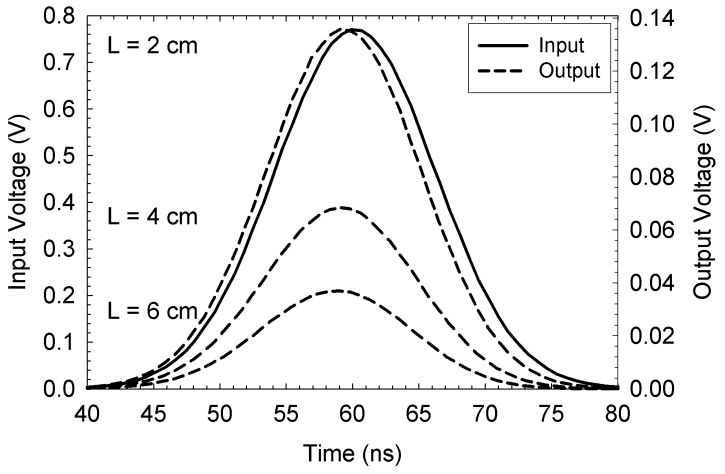

Fig. 10.16 Time-domain simulations showing negative group delay for the 2-cm, 4-cm, and 6-cm transmission lines, with delays of -0.89 ns, -1.17 ns and-1.53 ns, respectively.

point can be found elsewhere [8], a short justification can be provided by considering the following: Every causal signal has a starting point in time, before which the signal does not exist. This starting point is marked by a discontinuity in the pulse envelope or higher-order derivatives of the envelope, at which point the pulse is no longer analytic. These points of non-analyticity are the conveyers of *genuine information* and can be shown to propagate at exactly the speed of light c under all circumstances [8, 9, 23], and thereby fulfill the requirements of the relativistic causality. In short, for a smoothly varying pulse, presented by an analytical function, there is no more information in the pulse peak than in its earliest parts.

The propagation of these discontinuities can be examined using time-domain simulations as shown in Fig. 10.17. The discontinuities in the pulse waveform were established by introducing a "turning-on" point, commonly referred to as the front. The propagation of the front through the PLTLs of different lengths, having negative group delays, can be seen by examining the first 0.3 ns of the pulse evolution, shown on a logarithmic scale in Fig. 10.17. The output pulse fronts for the three structures all suffer the expected *positive luminal delays* with respect to the input fronts, given by L/c, where L is the length of the transmission line. Thus the simulations show that causality is preserved as seen by the fact that discontinuities in the pulse travel at exactly the speed of light in vacuum.

While the simulations indicate the causal propagation of information by the points of non-analyticity, the amplitudes associated with these fronts are particularly small, making their experimental detection a challenging task. This difficulty is one of the reasons that we practically detect a "signal" by observing its maximum or half-maximum points, which in turn can be made to propagate superluminally or with negative velocities.

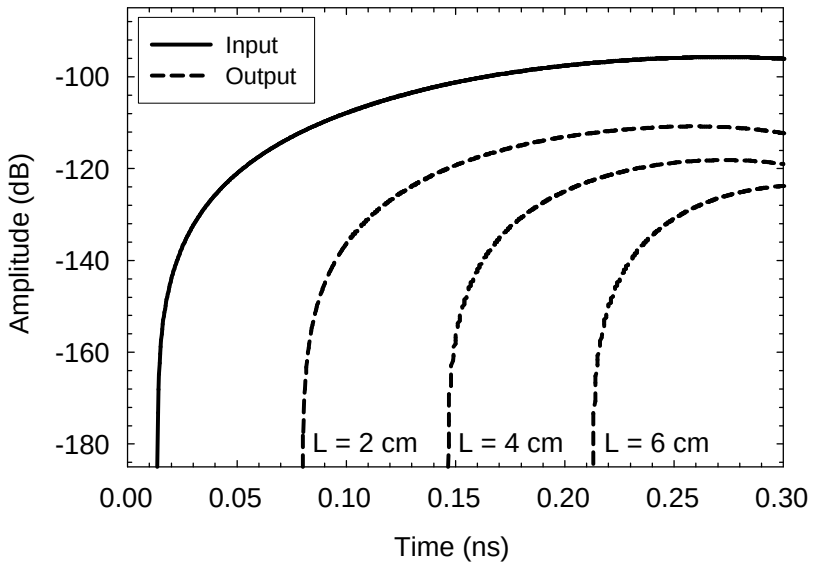

Fig. 10.17 Time-domain simulations of the modulated pulse fronts, plotted on a logarithmic (dB) scale. The input pulse front always precedes the output front by a time equal to L/c, where L is the length of the line. On the other hand (see Fig. 10.16), the output peak precedes the input peak.

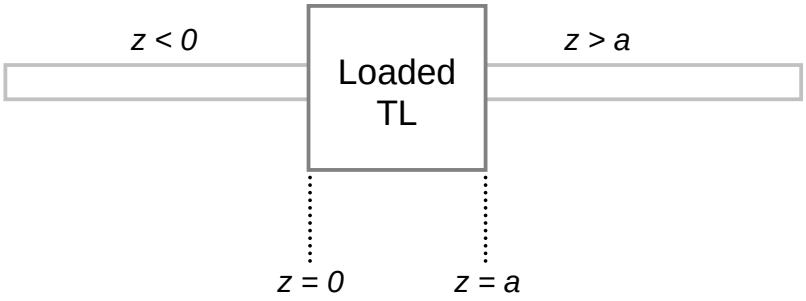

Fig. 10.18 A transmission line consisting of two regular lines ($z < 0$ and $z > a$) and a PLTL ($0 < z < a$) used for the simulations that explain the mechanism behind negative group delay.

10.4.4.3 Physical Mechanism Underlying Negative Group Delay The mechanism behind the pulse advancement can be also explained in terms of pulse reshaping. We can study the time evolution of a pulse by considering the spatio-temporal voltage distributions of the individual Fourier components making up the pulse. The system under study, shown schematically in Fig. 10.18, consists of two sections of regular transmission line occupying the regions $z < 0$ and $z > a$, surrounding a PLTL section of length a. The PLTL is assumed to be a transmission line of length 2 cm, having a dispersive behavior determined by the dispersion relation (10.21), and operated within the anomalous dispersion band. That is, the PLTL exhibits both negative refractive index and negative group velocity properties.

Consider a modulated Gaussian pulse, with center frequency in the anomalous dispersion band, excited on the $z < 0$ transmission line segment. By Fourier analysis, this waveform can be decomposed into many single-frequency sinusoidal components.

The peak of the pulse is formed at the position where these individual frequency components interfere constructively, and the nulls of the pulse are formed where these components interfere destructively.

The space- and time-dependent voltage distribution $V_n(z,t)$ for the n^{th} spectral component of the Gaussian pulse is given by:

$$V_n(z,t) = \begin{cases} G_n \cos(\omega_n t - k_n z) & z < 0 \\ G_n e^{-\alpha_n z} \cos(\omega_n t - \beta_n z) & 0 < z < a \\ G_n e^{-\alpha_n a} \cos(\omega_n t - k_n [z-a] - \beta_n a) & z > a \end{cases} \tag{10.25}$$

Here ω_n and G_n are the frequency and amplitude of the n^{th} harmonic, and is the propagation constant on the regular transmission line, in the regions $z < 0$ and $z > a$. In the PLTL section $0 < z < a$, the propagation and the attenuation constants of the n^{th} harmonic are β_n and α_n, respectively, calculated from the dispersion relation (10.21). Note that, according to (10.25), the peak of the pulse strikes the interface $z = 0$ at $t = 0$.

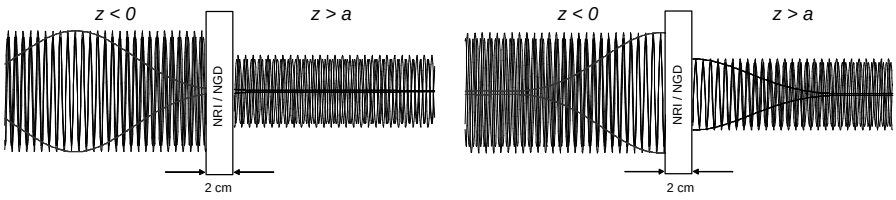

Fig. 10.19 Simulations illustrating the pulse-reshaping mechanism which underlies the negative group delay. (a) Three main frequency components of the Gaussian pulse and the resulting pulse envelope 13 ns before the input peak reaches the loaded transmission line interface. (b) The same three frequency components 0.5 ns before the input peak reaches the interface; at this point a peak has been already formed at the output.

Fig. 10.19(a) displays three spectral components of a Gaussian pulse with frequencies in the anomalous dispersion band at the instant $t = -13$ ns, calculated from (10.25). In addition to the underlying harmonics, Fig. 10.19(a) also displays the pulse envelope, so that the peak location can be clearly identified. It is evident from the figure that the frequency components add up in phase and a peak is formed in the $z < 0$ section of the transmission line.

As time progresses, the pulse propagates along the transmission line and the early part of the pulse encounters the PLTL section. By virtue of the phase compensation caused by the anomalous dispersion, the negative group delay transmission line rearranges the relative phases of the individual frequency components. Since the phase response of the line is approximately linear and the magnitude response is approximately flat over the bandwidth of the Gaussian pulse, the frequency components add up to produce a close copy of the original pulse, in the region $z > a$. This output pulse appears at $t = -0.5$ ns, before the input peak reaches the first interface, as shown in Fig. 10.19(b). Note that the output pulse amplitude is reduced in magnitude relative to the input pulse, though the envelope retains its basic shape. Figure 10.19(b) thus shows that the peak of the output pulse appears at the output terminal 0.5 ns before the input peak reaches the input terminal. Note that the effects of reflections from the interfaces in these simulations have been ignored. These reflections produce standing waves in the $0 < z < a$ section, and thus cause a further reduction in the transmitted pulse amplitude; however, they do not affect the location of the pulse peak.

10.4.5 PLTL Exhibiting Negative or Positive Phase and Group Delays - Time Domain Measurements

To verify our theoretical predictions, coplanar waveguides with 1, 2, 3 unit cells depicted in Fig. 10.9 were manufactured (recall that in our time-domain analysis the value of R_r is 150Ω. The experimental setup used to measure the group delay

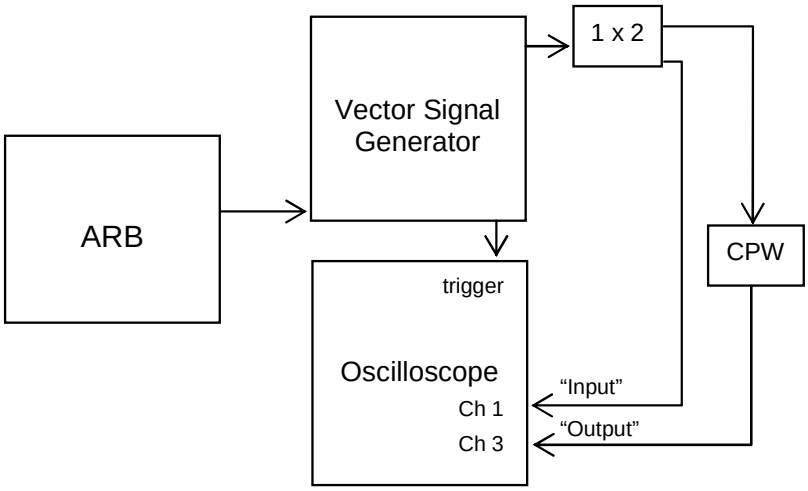

Fig. 10.20 Schematic diagram of the experimental setup used to measure negative group delay in the time-domain.

is schematically shown in Fig. 10.20. A base-band Gaussian pulse of temporal width 40 ns was created with a Tektronix AWG2041 arbitrary waveform generator (ARB), and modulated with a Rohde & Schwartz SMV03 vector signal generator at frequencies between 1.1 and 1.5 GHz. The modulated signal was then divided by a 1×2 splitter. Any discrepancy in length between the two cables joining the splitter to the oscilloscope will introduce an inherent delay between the two paths, thereby affecting the accuracy of the final group delay measurements. Therefore, both outputs of the splitter were initially connected to the Channels 1 and 3 of an Agilent 54846 Infiniium oscilloscope (bandwidth 2.25 GHz) for a calibration measurement. The delay was measured on the Infiniium scope and electronically equalized to 0 $\pm$ 0.1 ns, using the oscilloscope internal functions. After this calibration step, the CPW was inserted into the Channel 3 cable, as indicated in Fig. 10.20. In this way, both the input and output signal of the PLTL were simultaneously recorded on the oscilloscope.

Figure 10.21(a) shows the behavior of the 3-stage loaded transmission line operated at 1.11 GHz, in the band of positive group delay, that is, away from the anomalous dispersion band. For this case a positive group delay of approximately +1.5 ns, due to propagation along the 6-cm line, was observed. Under normal conditions, therefore, the peak of the output pulse appears at a later time than the peak of the input pulse. In contrast, Fig. 10.21(b) shows the input and output pulses when the PLTL is operated within the anomalous dispersion band, at the resonance frequency of 1.27 GHz, where a negative group delay of -3.1 ns was measured. Note that in Fig. 10.21(b) the output peak precedes the input peak; this unusual outcome is the meaning of negative group delay.

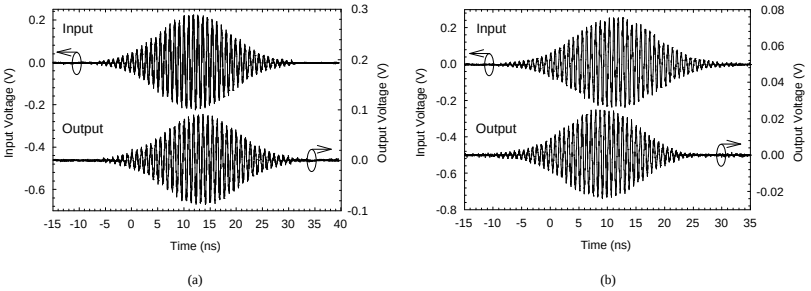

Fig. 10.21 Time-domain experimental results for the 3-stage negative delay circuit at two frequencies. (a) Positive delay at a center frequency of 1.11 GHz, 160 MHz below resonance. (b) Negative group delay at the resonance frequency of 1.27 GHz.

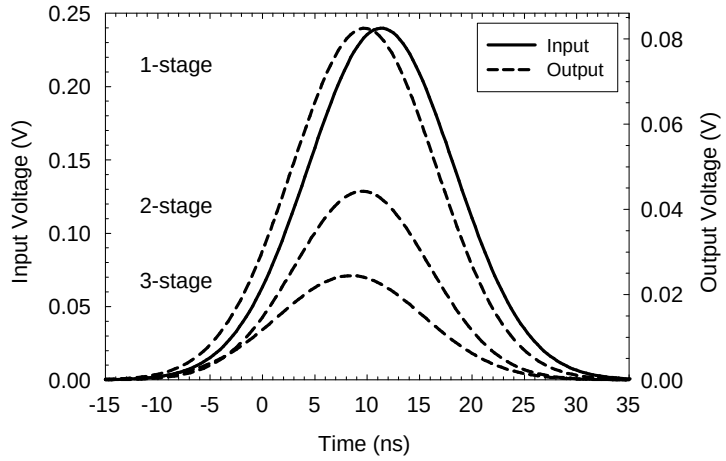

Fig. 10.22 Experimental results showing extracted pulse envelopes for the 1-, 2- and 3-stage transmission lines, with delays of -1.6 ns, -1.9 ns, and -3.1 ns, respectively.

Figure 10.22 shows the measured input pulse (solid curve) and output pulses (dashed curves) at the point of maximum negative group delay, approximately 1.27 GHz, for the 1-, 2- and 3-stage circuits. For clarity, only the pulse envelopes are shown. These curves are the experimental validation of Fig. 10.16. The envelopes were extracted from the raw data by fitting a three-parameter Gaussian curve. The peak arrival times were acquired from the Gaussian fit parameters to within $\pm$ 0.2 ns. At the $R_r L_r C_r$ resonance frequency, the 1-, 2- and 3-stage circuits exhibit group delays of -1.6 ns, -1.9 ns and -3.1 ns, respectively. Note that, as expected, the greatest negative delay and the greatest attenuation are found for the longest transmission line, and the least negative delay and least attenuation for the shortest line.

In comparing Figs. 10.16 and 10.22 the trend that longer lines have greater negative delay and greater insertion loss is common to both simulation and experiment; however, there are also some discrepancies. For example, there is generally less attenuation and more pulse advancement in the experiments. These discrepancies are due to the differences between the components used in the simulations and those in the actual devices. First, nominal values for the components were used in the simulations. In practice, however, the components have manufacturer stated [5] tolerances of $\pm$ 5%. By including these tolerances in our simulations, we found that the discrepancies between the measured and calculated group delay can be reduced by half. The group delay is particularly sensitive to changes in the resistor or capacitor in the $R_rL_rC_r$ resonator, and variation in these component values will affect the slope of the transmission phase, thus altering the amount of negative group delay. Second, and more importantly, the simulations use ideal component models, and thus the self-resonant behaviors of the capacitors and inductors were not included. In practice, the self-resonances can change the overall impedance of the $R_rL_rC_r$ resonator and hence altering the device attenuation and negative group delay. These two effects may be included in the simulations if measured S-parameters are used for each component, a tedious but effective method of improving the agreement between experiment and simulation.

10.5 CONCLUSIONS

In this Chapter we have studied the dynamics of wave propagation in a general medium having both an effective negative refractive index and a negative group velocity. Our study was motivated by our desire to control the dispersive effects such as phase velocity, group velocity, and group velocity dispersion in general, and the associated signs of the first two effects in particular.

We began our studies by formulating equivalent ways of describing the aforementioned dispersive effects in terms of the phase index and its higher order derivatives, or more generally by formulating these effects in terms of various delays such as phase delay, group delay, group delay dispersion, and so on. Our attention has been focused on the phase and group delays and their associated signs, leaving the remaining dispersive terms for later considerations.

We then proceeded to discuss the concept of abnormal group velocities for which the group velocity can become superluminal (exceeding the speed of light in vacuum) or

[5] As alluded to in Sec. 10.4.3, the actual tolerance may well be above the manufacturer stated values.

negative, without violating the principles of relativistic causality. This then served as a conduit to bring together the two notions of negative phase and negative group velocities (negative phase and negative group delays) in structures that can exhibit both behaviors in addition to normal wave propagation (positive phase and group velocities) or backward waves (negative phase but positive group velocities.)

We continued our analysis with the case of a single slab possessing Lorentzian electric and magnetic responses. This case was chosen for both its generality and simplicity. We theoretically showed that such a medium can support both negative phase and group velocities.

We then considered a practical periodically-loaded transmission line (PLTL) to demonstrate some of the above theoretical considerations. A CPW transmission-line was periodically loaded with series capacitor and shunt inductor in addition to a resonant RLC circuit such that the overall transmission line exhibited positive or negative phase velocity and positive or negative group velocity depending of the exact combination. Assuming an infinitely long PLTL, the structure was studied using periodic analysis. For a finite length structure, the scattering matrix formulation was used to calculate the medium's response. The theoretical findings were further confirmed using frequency-domain measurements. We also performed theoretical and experimental studies of our PLTL in the time-domain. It was observed that such a medium can be made to operate with both negative phase and group delays (negative phase and group velocities) for which the output peak envelope precedes the input peak.

Acknowledgments

The authors would like to thank their students who have contributed to the present work, in particular Suzanne J. Erickson, Omar F. Siddiqui, Jonathan Woodley, and Mark Wheeler. This work was supported by the Natural Sciences and Engineering Research Council of Canada under Grant RGPIN 249531-02, and by the Photonics Research Ontario under Project 03-26, and with the funds provided by the Canada Foundation for Innovation and Ontario Innovation Trust.

REFERENCES

1. V. G. Veselago, "Properties of Materials Having Simultaneously Negative Values of the Dielectric ϵ and the Magnetic μ Susceptibilities," *Soviet Physics-Solid State*, vol. 8, pp. 2854-2856, 1967.

2. V. G. Veselago, "The Electrodynamics of Substances with Simultaneously Negative Values of ϵ and μ ," *Soviet Physics USPEKHI*, vol. 10, no. 4, pp. 509-514, Jan.-Feb. 1968.

3. R. A. Shelby, D. R. Smith, S. Schultz, "Experimental verification of a negative index of refraction," *Science*, vol. 292, pp. 77-79, 2001.

4. D. R. Smith, W. J. Padilla, D. C. Vier, S. C. Nemat-Nasser, S. Schultz, "Composite medium with simultaneously negative permeability and permittivity" *Physical Review Letters*, vol. 84, pp. 4184-4187, 2000.

5. R. Y. Chiao and A. M. Steinberg, "Tunneling Times and Superluminality," *Progress in Optics*, vol. 37, pp. 345-405, 1997.

6. A. M. Steinberg, P. G. Kwiat, and R. Y. Chiao, "Measurement of the single-photon tunneling time" *Physical Review Letters*, vol. 71, pp. 708-711, 1993.

7. M. Mojahedi, E. Schamiloglu, K. Agi, and K. J. Malloy, "Frequency Domain Detection of Superluminal Group Velocities in a Distributed Bragg Reflector" *IEEE Journal of Quantum Electronics*, vol. 36, pp. 418-424, 2000.

8. M. Mojahedi, E. Schamiloglu, F. Hegeler, and K. J. Malloy, "Time-domain detection of superluminal group velocity for single microwave pulses," *Physical Review E (Statistical Physics, Plasmas, Fluids, and Related Interdisciplinary Topics)*, vol. 62, pp. 5758-5766, 2000.

9. M. Mojahedi, K. J. Malloy, G. V. Eleftheriades, J. Woodley, and R. Y. Chiao, "Abnormal wave propagation in passive media," *IEEE Journal of Selected Topics in Quantum Electronics*, vol. 9, pp. 30-39, 2003.

10. G. B. Arfken, *Mathematical Methods for Physicists*, 3rd ed. Orlando: Academic Press, 1985.

11. J. D. Jackson, *Classical Electrodynamics*, 3rd ed. New York: Wiley, 1998.

12. A. Papoulis, *The Fourier Integral and its Applications*. New York: McGraw-Hill, 1962.

13. H. M. Nussenzveig, *Causality and Dispersion Relations*. New York: Academic Press, 1972.

14. S. Ramo, J. R. Whinnery, and T. Van Duzer, *Fields and Waves in Communication Electronics*, 3rd ed. New York; Toronto: Wiley, 1994.

15. G. V. Eleftheriades, A. K. Iyer, P. C. Kremer, "Planar negative refractive index media using periodically L-C loaded transmission lines," *IEEE Transactions on Microwave Theory and Techniques*, vol. 50, pp. 2702-2712, Dec. 2002.

16. M. Notomi, "Theory of light propagation in strongly modulated photonic crystals: Refractionlike behavior in the vicinity of the photonic band gap," *Physical Review B (Condensed Matter)*, vol. 62, pp. 10696-10705, 2000.

17. R. Marques, J. Martel, F. Mesa, and F. Medina, "Left-handed-media simulation and transmission of EM waves in subwavelength split-ring-resonator-loaded metallic waveguides," *Physical Review Letters*, vol. 89, pp. 183901/1-4, 2002.

18. E. L. Bolda, R. Y. Chiao, and J. C. Garrison, "Two theorems for the group velocity in dispersive media," *Physical Review A*, vol. 48, pp. 3890-3894, 1993.

19. E. L. Bolda, J. C. Garrison, and R. Y. Chiao, "Optical Pulse-Propagation At Negative Group Velocities Due to a Nearby Gain Line," *Physical Review A*, vol. 49, pp. 2938-2947, 1994.

20. L. J. Wang, A. Kuzmich, and A. Dogariu, "Gain-assisted superluminal light propagation," *Nature*, vol. 406, pp. 277-279, 2000.

21. M. D. Stenner, D. J. Gauthier, and M. A. Neifeld, "The speed of information in a 'fast-light' optical medium," *Nature*, vol. 425, pp. 695-698, 2003.

22. J. Woodley and M. Mojahedi, "Negative group velocity in left-handed materials," presented at 2003 *IEEE International Symposium on Antennas and Propagation: URSI North American Radio Science Meeting*, Columbus, OH, USA, 2003.

23. L. Brillouin, *Wave Propagation and Group Velocity*. New York: Academic Press, 1960.

24. L. Brillouin, *Wave Propagation in Periodic Structures; Electric Filters and Crystal Lattices*, 1st ed. New York; London: McGraw-Hill Book Company inc., 1946.

25. M. Born and E. Wolf, *Principles of Optics*, 4th ed. Oxford, New York,: Pergamon Press, 1970.

26. L. D. Landau, E. M. Lifshittz, and L. P. Pitaevski, *Electrodynamics of Continuous Media*, 2nd , rev. and enl. / ed. Oxford [Oxfordshire]; New York: Pergamon, 1984.

27. C. G. B. Garrett and D. E. McCumber, "Propagation of a Gaussian Light Pulse Through an Anomalous Dispersion Medium," *Physical Review A*, vol. 1, pp. 305-313, 1970.

28. S. Chu and S. Wong, "Linear Pulse-Propagation in an Absorbing Medium," *Physical Review Letters*, vol. 48, pp. 738-741, 1982.

29. A. Ranfagni, D. Mugnai, P. Fabeni, and G. P. Pazzi, "Delay-Time Measurements in Narrowed Wave-Guides As a Test of Tunneling," *Applied Physics Letters*, vol. 58, pp. 774-776, 1991.

30. A. Enders and G. Nimtz, "Photonic-Tunneling Experiments," *Physical Review B*, vol. 47, pp. 9605-9609, 1993.

31. A. Ranfagni, P. Fabeni, G. P. Pazzi, and D. Mugnai, "Anomalous Pulse Delay in Microwave Propagation : a Plausible Connection to the Tunneling Time," *Physical Review E*, vol. 48, pp. 1453-1460, 1993.

32. P. Balcou and L. Dutriaux, "Dual Optical Tunneling Times in Frustrated Total Internal-Reflection," *Physical Review Letters*, vol. 78, pp. 851-854, 1997.

33. D. Mugnai, A. Ranfagni, and L. Ronchi, "The Question of Tunneling Time Duration : a New Experimental Test At Microwave Scale," *Physics Letters A*, vol. 247, pp. 281-286, 1998.

34. R. Y. Chiao and J. Boyce, "Superluminality ; Parelectricity ; and Earnshaws Theorem in Media With Inverted Populations," *Physical Review Letters*, vol. 73, pp. 3383-3386, 1994.

35. R. A. Shelby, D. R. Smith, S. C. Nemat-Nasser, and S. Schultz, "Microwave transmission through a two-dimensional, isotropic, left-handed metamaterial," *Applied Physics Letters*, vol. 78, pp. 489-91, 2001.

36. D. R. Smith, N. Kroll, "Negative refractive index in left-handed materials," *Physical Review Letters*, vol. 85, pp. 2933-2936, Oct. 2000.

37. D. M. Pozar, *Microwave Engineering*, 2nd ed. New York: Wiley, 1998.

38. R. E. Collin, *Foundations for Microwave Engineering*, 2nd ed. New York; Montreal: McGraw-Hill, 1992.

39. O. Siddiqui, M. Mojahedi, S. Erickson, and G. V. Eleftheriades, "Periodically loaded transmission line with effective negative refractive index and negative group velocity," presented at 2003 *IEEE International Symposium on Antennas and Propagation: URSI North American Radio Science Meeting*, Columbus, OH, USA, 2003.

40. O. F. Siddiqui, M. Mojahedi, and G. V. Eleftheriades, "Periodically loaded transmission line with effective negative refractive index and negative group velocity," *IEEE Transactions on Antennas and Propagation*, vol. 51, pp. 2619-25, 2003.

41. O. F. Siddiqui, S. J. Erickson, G. V. Eleftheriades, and M. Mojahedi, "Time-Domain Measurement of Negative Group Delay in Negative-Refractive-Index Transmission-Line Metamaterials," *IEEE Transactions on Microwave Theory and Techniques*, vol. 52, pp. 1449-1454, 2004.

Index